ELSEVIER

Contents lists available at ScienceDirect

Fuel Communications

journal homepage: www.sciencedirect.com/journal/fuel-communications



Community microgrid: Control structure, design, and stability

Oindrilla Dutta¹, Ahmed Mohamed^{2,*}

Smart Grid Interdependencies Laboratory, The City University of New York, City College, New York, NY, United States

ARTICLE INFO

Keywords: Community microgrid DER Distribution network Primary controller Power transfer Transient stability

ABSTRACT

This work investigates the performance of a community microgrid (C-µGrid) in an islanded mode of operation. A control structure has been developed, which focuses on transient stability of the primary controllers (PCs) of individual distributed energy resources (DERs) in the community, and also when the DERs work in tandem to balance load and generation. This approach shows a method for decoupling the state vectors of a highly coupled system, so that the system parameters can be regulated separately with accuracy, speed and stability. This work also demonstrates a technique for analysing and minimizing the impact of communication delays, which may exist between two controllers at different hierarchies. Besides, our analysis shows that power transferred between the multiple buses of a C-µGrid causes voltage variation that is different from traditional power distribution. Accordingly, a power transfer method has been proposed. These aforementioned control designs have been modeled for a C-µGrid structure that forms part of a modified IEEE 13 bus system, and simulated in real-time using OPAL-RT. A comparative analysis has been performed between DER voltage references provided by traditional optimal power flow (OPF) and our proposed method of power transfer. The simulation results show stable system operation during normal condition, and post delay recovery, when our developed control and power transfer methods are used. However, certain combinations of voltage references provided by OPF destabilizes the PCs and degrades the quality of power injection into the grid. These results have been utilized to characterize the functional requirements of a C-µGrid Central/Distributed Controller.

1. Introduction

DERs are essential alternatives to fossil fuel in our effort towards obtaining clean energy. An architecture in which DERs are managed to operate in both grid-connected mode and islanded mode is referred to as a Microgrid [1–3]. Microgrids provide sustainability and resiliency to the utility grid [4,5] by enabling a high penetration of DERs. However, the implementation and operating cost of microgrid is high, rendering a trade-off between cost and reliability.

Urban areas are major consumers of electricity that are characterised by limited space, and hence distribution cables are often underground. As a result, urban power distribution networks remain immune to low frequency high impact events at the transmission level. This poses an opportunity for the distribution network to isolate itself from the transmission system, and form a network of microgrids leveraging the existing distribution infrastructure (Fig. 1). Such a structure is called C- μ Grid, which helps in reduction of typical microgrid costs and

limitations (e.g, space) by sharing cost and resources [6,7]. Some existing C- μ Grid projects around the world, comprising different load carrying capacities and combinations of DERs, are reported in [8–10].

 $C-\mu$ Grid comprises multiple stakeholders with unique operation and management objectives, where the control objectives of individual DERs vary during grid-connected mode and emergency islanding mode. Hence, a hierarchy of control protocol is essential for achieving the common goals of sustainability, resiliency and cost [11]. At the lowest level in this hierarchy, primary controllers (PCs) regulate the power electronic converters of DERs locally. At the next level, a secondary $C-\mu$ Grid central/distributed controller ($C-\mu$ Grid-C/D-C) is required to provide set-points to these PCs for optimizing control objectives that encompass generation and load balance, battery management with provision for emergency, and decision to connect or isolate from the main grid. This controller must communicate with a higher tertiary level controller, which is a distribution management system [12].

In the existing literature, different algorithms for designing the C-

E-mail address: amohamed@ccny.cuny.edu (A. Mohamed).

^{*} Corresponding author.

¹ Member, IEEE

² Senior Member, IEEE



Fig. 1. An overview of distribution network with provision for C-µGrid.

μGrid-C/D-C have been proposed, with a focus on energy management and trading [13–15]. These studies analyze the business aspect of power sharing by the multiple microgrids such that the cost of power transfer is optimized. These studies, however, are based on assumptions of transient and steady-state stability of the PCs. This is predominantly because there exists extensive research on design and stability of PCs for parallel operation of DERs [16,17]. However, these designs cannot be extrapolated to the C-µGrid concept because the loads and DERs are shared among multi-points of coupling instead of a single point of common coupling (PCC). Therefore, voltage and angle are no longer the common global variables, rendering popular methods like $P - \delta$, Q - V droop [18–20] ineffective. Besides, because of the physical distance between the multiple microgrids and loads, the C-µGrid-C/D-C must rely on communication infrastructure for receiving measurements from the system and sending control actions to the PCs. This poses possibility for signal degradation due to communication latency, thereby impacting the transient stability of a C- μ Grid.

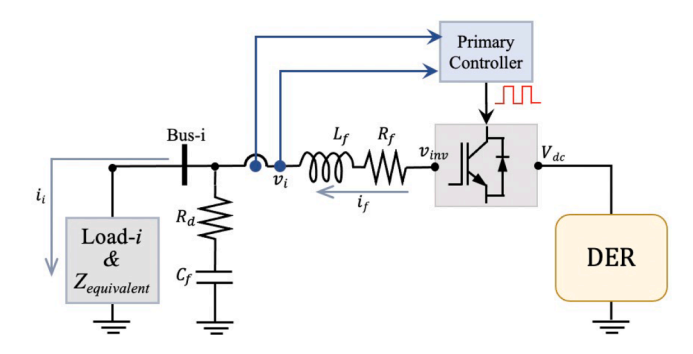


Fig. 2. Overview of control parameters of individual DERs.

In this work, we have highlighted the vulnerabilities of a C- μ Grid in islanded mode of operation and proposed a control approach for improved system performance. The contributions of this work are: 1) Design methods for voltage and current controllers so that those are stable against load variation while ensuring fast response and quality signal injection; 2) A technique for incorporating the impact of delays, between the PCs and C- μ Grid-C/D-C, into the control analysis, and minimize its impact on the transient stability of a C- μ Grid; 3) A procedure for evaluating the power transferred from source to sink, as a function of increased loading, by considering the dynamics of the renewable energy resources. This is essential for determining the receiving end voltage profile. These design methods have been tested in a C- μ Grid that forms part of a modified IEEE-13 bus system. A detailed model of this system has been simulated in a real-time testbed using OPAL-RT.

$$\begin{bmatrix} \dot{x}_{1k} \\ \dot{x}_{2k} \\ \dot{x}_{3k} \\ \dot{x}_{4k} \end{bmatrix} = \begin{bmatrix} 0 & 1 & 0 & 0 & 0 & 0 & 0 \\ -\frac{1}{C_{fk}} \left[\frac{1}{L_{fk}} + \frac{1}{L_{i}} \right] & 0 & 0 & \omega & \frac{\varepsilon m_{a-k}}{L_{fk} C_{fk}} & \frac{R_{i}}{C_{fk} L_{i}} & 0 \\ 0 & 0 & 0 & 1 & 0 & 0 & 0 \\ 0 & -\omega & -\frac{1}{C_{fk}} \left[\frac{1}{L_{fk}} + \frac{1}{L_{i}} \right] & 0 & 0 & 0 & \frac{R_{i}}{C_{fk} L_{i}} \end{bmatrix} \begin{bmatrix} x_{1k} \\ x_{2k} \\ x_{3k} \\ x_{4k} \\ x_{7k} \end{bmatrix} + \begin{bmatrix} 0 & 0 \\ -\frac{R_{fk}}{C_{fk} L_{fk}} & 0 \\ 0 & 0 \\ 0 & -\frac{R_{fk}}{C_{fk} L_{fk}} \end{bmatrix} \begin{bmatrix} u_{1k} \\ u_{2k} \end{bmatrix}$$

$$(1)$$

$$v_{dk-i} = \frac{\left(sL_{jk} + R_{jk}\right)}{s^{2}L_{jk}K_{VP} - s\left[e^{s\tau} - \left(R_{jk}K_{VP} - L_{jk}K_{VI}\right)\right] + R_{jk}K_{VI}} \begin{bmatrix} sK_{VP} + K_{VI} & 0 & 0 & 0\\ 0 & -s\omega C_{jk} & 0 & 0\\ 0 & 0 & s & 0\\ 0 & 0 & 0 & \frac{se^{s\tau}}{sL_{jk} + R_{jk}} \end{bmatrix} \begin{bmatrix} v_{dk-i}^{*}\\ v_{dk-i}\\ i_{d-i}\\ v_{d-inv} \end{bmatrix}$$

$$(2)$$

Fig. 3. Block diagram of voltage control.

2. C-µGrid structural design

The structural layout of a C- μ Grid entails a design approach that ensures stability for both individual microgrids, and when multiple microgrids work in tandem to share loads. In this section, a hierarchy for the PCs of the C- μ Grid in islanded mode and their design have been proposed, along with the determination of stability margins. This C- μ Grid consists of N number of buses with K number of DERs. Fig. 2 shows the connection of the kth DER to the ith bus. In the absence of a grid and other power sources, this DER must maintain the voltage at that bus and its connected buses, while supplying the loads. Thus, the control design must ensure stability of frequency, voltage and current within a wide variation of loads. In conventional methods, both the voltage and current controllers are designed by considering only the inverter filter as the plant to be controlled. However, the following analysis demonstrates the vulnerability of the bus voltage to filter design, while that of the current to the equivalent impedance seen by the inverter at the PCC.

2.1. Design of voltage controller (VC)

In a C- μ Grid, due to small $\frac{X}{K}$ ratio, the transfer of power from one bus to another is primarily dependent on voltage difference between the buses. Hence, considerable accuracy in tracking reference signals is the primary feature of the VC. The measured $3-\phi$ voltage (v_i) across the filter capacitor (C_f) , after Park Transformation, is regulated by the VC by modulating the filter current $(i_{f-d/q})$. The direct-axis (v_{d-i}) and quadrature-axis (v_{q-i}) voltages are functions of the load current $(i_{d/q-i})$, and the inverter output voltage (v_{inv}) . Besides, v_{inv} depends on the DC voltage (V_{dc}) of a DER, which varies with the state of charge in a battery or solar irradiace in a PV system. Thus, the states, input, output and control variables of the system in Fig. 2 are defined as follows and the corresponding state equation is shown in (1).

$$v_{d-i} \rightarrow x_1 \text{ and } y_1, \dot{x_1} = dx_1/dt = x_2, v_{q-i} \rightarrow x_3 \text{ and } y_2, \dot{x_3} = dx_3/dt = x_4, \ i_{fd} \rightarrow u_1, \ i_{fq} \rightarrow u_2, \ V_{dc} \rightarrow x_5, \ i_{d-i} \rightarrow x_6, \ i_{q-i} \rightarrow x_7.$$

The system dynamics represented by (1) show that the regulation of $v_{d/q-i}$ is a multiple input multiple output (MIMO) control problem. Fig. 3 illustrates the block diagram for controlling v_d , while a similar approach has also been adopted for v_q . The multiple inputs for controlling v_d are the reference signal (v_d^*) , v_q across the filter capacitor, the current through the load impedance at the ith bus $(R_i + j\omega L_i)$, and v_{inv} . Here, plant of the VC is the filter circuit $|R_f + sL_f|$, and the control signal is i_{f-d}^* .

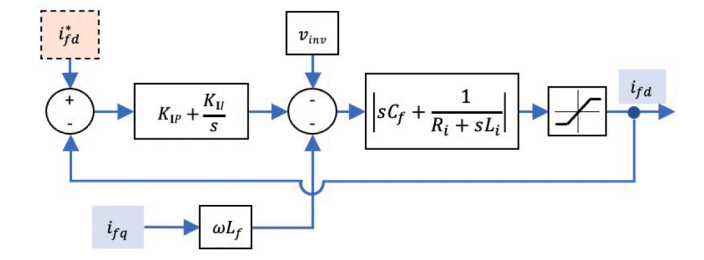


Fig. 4. Block diagram of current control.

In order to study the impact of communication latency between the feedback signal for voltage measurement at the ith bus and the C- μ Grid-C/D-C, a delay of time duration τ has been represented as $e^{-s\tau}$. The position of this delay in the block diagram of VC is crucial for proper analysis of its impact [21,22]. The delay affects the error between v_d^* and v_d , as well as v_q and the load current. However, v_{inv} is independent of this, and hence the delay block is positioned prior to the control signal (Fig. 3). The other feedback signal with transfer function K(s), from v_d to i_{fd}^* , is a provision for reducing any destabilizing effect of a delay. The transfer function of K(s) is system specific and therefore has been elaborated in Section 4.1, where a case study has been discussed.

The coupling matrix pertaining to Fig. 2 is shown in (2), where the control objective is to reduce the coupling effect of the other inputs so that v_d can accurately follow v_d^* . If the plant transfer function of the system is G(s) and that of the PI controller is $K_{PI}(s)$, then the coupling phenomenon can be summarised as follows:

$$v_d = \frac{GK_{PI}}{1 + GK_{PI}} v_d^* - \frac{s\omega C_f G}{1 + GK_{PI}} v_q + \frac{sG}{1 + GK_{PI}} i_d + \frac{1}{1 + GK_{PI}} v_{inv}, \text{ such that}$$
(3)

$$\lim_{K_{PI}\to\infty} \mathbf{v_d} = [\mathbf{I}] * \mathbf{v_d}^* + 0 + 0 + 0$$

However, very high values of PI gains can make the system unstable, therefore, a compatibility between the filter parameters in G(s) and the gains in $K_{PI}(s)$ must be achieved. This is demonstrated with eigenvalues in Section 4.1. The VC provides current references, $i_{f-d/q}^*$, to the current controller.

$$i_{fd-k} = \frac{\left(C_{fk}L_{i}s^{2} + C_{fk}R_{i}s + 1\right)}{\left(C_{fk}L_{i}s^{2} + C_{fk}R_{i}s + 1\right)\left(sK_{IP} + K_{II}\right) - \left(L_{i}s^{2} + R_{i}s\right)} \begin{bmatrix} \left(sK_{IP} + K_{II}\right) & 0 & 0\\ 0 & -\omega L_{fk}s & 0\\ 0 & 0 & s \end{bmatrix} \begin{bmatrix} i_{fd-k}^{*}\\ i_{fq-k}\\ v_{d-inv} \end{bmatrix}$$

$$(4)$$

2.2. Design of current controller (CC)

The CC is responsible for tracking the references provided by the VC and hence, its response time must be faster than that of the VC. Errors between $i_{f-d/q}^*$ and the current measurement signals $i_{f-d/q}$, after being transformed to their $3-\phi$ equivalent (Δi_{f-abc}), is passed through a PWM generator, which provides the necessary switching signals for operating the inverter. Thus, alteration of magnitude of Δi_{f-abc} presents amplitude modulation (m_a), which fundamentally causes the exchange of energy between a DER and load or multiple DERs.

A block diagram for controlling i_{f-d} is shown in Fig. 4, and a similar approach has been adopted for i_{f-q} . This figure shows that the CC takes into account the dynamics of the load impedance and filter capacitor, $\left|sC_f + \frac{1}{R_i + s\omega L_i}\right|$, into the plant transfer function. The advantage of this method is that the PI gains $(K_{IP} \text{ and } K_{II})$ can be tuned based on the size of each DER, so that the impact of load variation on system performance is minimized, without overdamping the system response. This ensures fast response of the CC and its stability over a desirable variation of loads, which is crucial for a C- μ G in islanded mode. A saturation limit has been provided to the tracking signal so that the amplitude modulation is bound within its linear zone.

The coupling matrix corresponding to Fig. 4 is presented in (4), which shows the dependence of i_{f-d} on the reference input (i_{f-d}^*) , measured quadrature axis current through the filter (i_{f-q}) and v_{inv} . Similar to the VC, the control objective here is to reduce the coupling of i_{f-d} with inputs i_{f-q} and v_{inv} , so that it can accurately track i_{f-d}^* . Besides, the relative position of the eigenvalues pertaining to (4) and (2) is crucial for making the CC faster than the VC.

2.3. Power transfer

In a $C-\mu G$ during its islanded mode of operation, the lack of rotational inertia due to absence of synchronous generators may cause faster voltage collapse/rise during power transfer. Thus, it is crucial to incorporate the dynamics of DERs, power electronic converters and their controllers into the conventional analysis for power transfer from a source to a sink.

Similar to the previous discussions, a DER is connected to bus number i and this DER number is k. Bus number n is connected to the DER bus i and contains a load Z_n . Then the voltage at the nth bus, due to power transfer by the kth DER is given by (5). The amplitude modulation, \mathbf{m}_{a-k} , of the inverter connected to the kth DER is a function of the load current, based on our VC and CC design in Sections 2.1 and 2.2. Besides, the relation between V_i and m_{a-k} follows a saturation nonlinearity for a constant V_{dc} [23]. In the following equation, Z_f and ψ_f are the impedance and angle of the inverter filter, respectively. Z_{i-n} and θ are, respectively, the impedance and angle of the the transmission line connecting bus i with bus n. ψ is the angle of the load Z_n . ε is a constant that varies with the type of PWM generator used by the CC, such as square wave PWM or sinusoidal PWM and so on.

$$V_{n} = \frac{Z_{n}\varepsilon \mathbf{m}_{a-k}V_{dc-k}}{\xi_{k}}, \forall n \in n_{k} \subset N,$$
where, $\xi_{k} = \sqrt{Z_{f}^{2} + \xi_{n}^{2} + 2Z_{f}\xi_{n}\cos(\psi_{f} - \zeta_{n})},$

$$\xi_{n} = \sqrt{Z_{n}^{2} + Z_{i-n}^{2} + 2Z_{n}Z_{i-n}\cos(\theta - \phi)}, i \subset N \& i \neq n$$
and $\zeta_{n} = \tan^{-1}\left(\frac{Z_{n}\sin\phi + Z_{i-n}\sin\theta}{Z_{n}\cos\phi + Z_{i-n}\cos\theta}\right)$

$$(5)$$

The active power transferred from the kth DER to the load Z_n can be represented by (6). The variation of active power with increment in load impedance, and the subsequent voltage profile is essential for

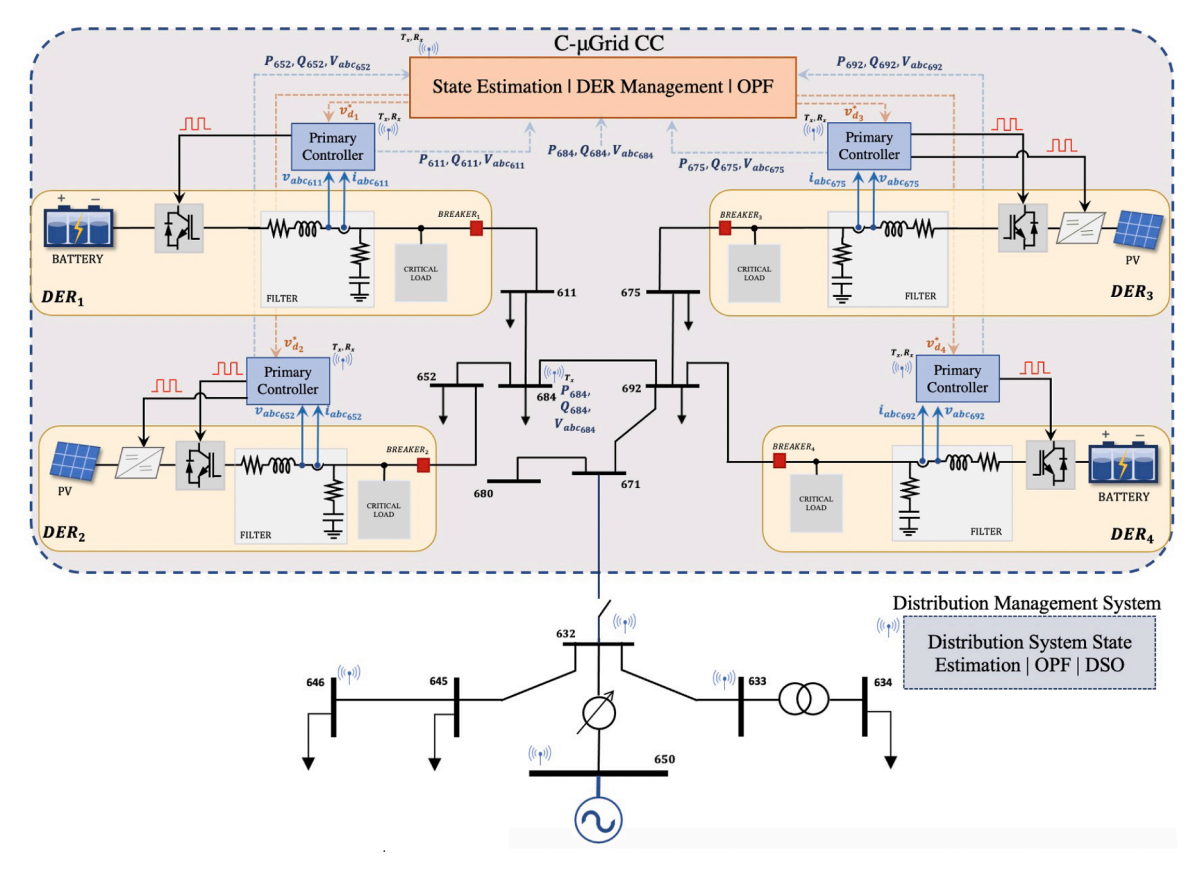


Fig. 5. A modified IEEE 13-bus system with $C-\mu$ Grid.

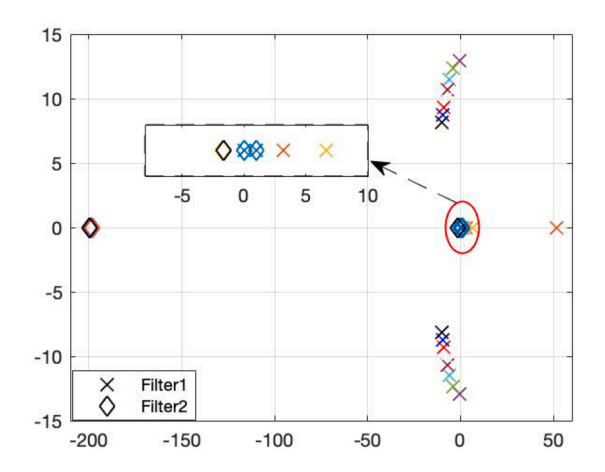


Fig. 6. Eigenvalues corresponding to voltage controller for different combinations of proportional and integral gain.

determining a stability margin.

$$P_{n} = \varepsilon^{2} Z_{n} \left(\frac{\mathbf{m}_{a-k} V_{dc-k}}{\xi_{k}} \right)^{2} \cos \zeta_{k}, \forall n \in n_{k} \subset N$$
where, $\zeta_{k} = \tan^{-1} \left(\frac{Z_{f} \sin \psi + \xi_{n} \sin \zeta}{Z_{f} \cos \psi + \xi_{n} \cos \zeta} \right)$
(6)

This proposed power transfer method is called C-µG Power Transfer (CMPT) and Section 4.3 provides further details with specific case study.

3. System under study

In this work, a modified IEEE 13 bus system, illustrated in Fig. 5, has been used as case study. The system comprises four DERs, each having different active (P_k) and reactive power (Q_k) sharing capacities, connected to four different buses. The DERs along with some of the loads and buses of the 13-bus system constitute a C- μ Grid. The C- μ Grid can island itself from the main grid by opening the breaker between Buses 671 and 632. Based on their power sharing capabilities, the DERs are provisioned to support the loads at their own buses and also the loads at other connected buses. Besides, these DERs can also island themselves from the C- μ Grid, with their critical loads, in the event of failures.

The 13-bus system is operated by a distribution management system, with functionalities like Distribution System State Estimation (DSSE), and Optimal Power Flow (OPF), that are utilized by a distribution system operator (DSO) for providing reliable distribution services and coordinating with transmission system operator (TSO). Since the C- μ Grid can island itself from the main grid, its resources must be managed using a secondary controller, which in this case is the C- μ Grid Central Controller (C- μ Grid-CC). C- μ Grid-CC receives the states (voltage, active

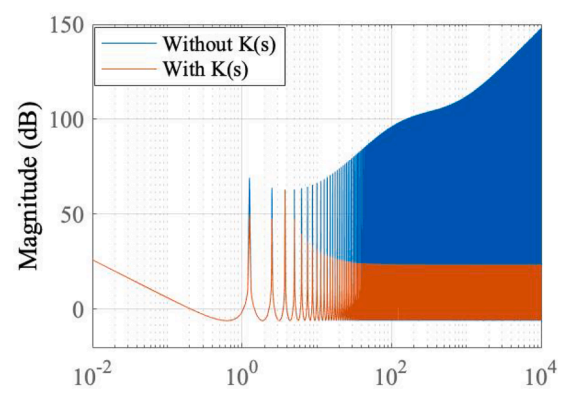


Fig. 7. Magnitude versus frequency plot for $\tau = 5$ s.

and reactive power) of some of the buses in the $C-\mu$ Grid, and determines the voltage set points of the PCs. This work focuses on the design of the PCs and their stability limits, which forms the basis of the functional requirements for the secondary controller.

4. Stability and sensitivity of controllers

In this section, the control design methods from Section 2 have been applied to the C- μ Grid in our aforementioned case study. The following analysis elaborates the stability and sensitivity of the controllers for DER_1 , that is connected to Bus. no. 611. Thus, k=1, i=611 and n=684. Similar results have also been obtained for the other DERs.

4.1. Voltage control and transient stability

Fig. 6 shows the eigenvalues of the VC, represented by the coupling equation in (2), with $\tau=0$. These eigenvalues pertain to two sets of values for filters R_{f1} and L_{f1} , and magnitude of the gains K_{VP} and K_{VI} have been increased from a minimum to a maximum. The figure shows that for Filter1 the eigenvalues shift to the left of the imaginary axis with increasing gains of K_{VP} and K_{VI} , however, the eigenvalues for Filter2 do not vary with the change in PI gains. Besides, the dominant eigenvalues corresponding to Filter2 are more stable than those of Filter1. Thus, Filter2 has been chosen for DER_1 along with $K_{VP}=2000$ and $K_{VI}=20000$, such that v_{d-1} follows v_{d-1}^* and is decoupled from the other inputs without over-damping the system.

When $\tau \neq 0$, magnitude oscillations occur at higher frequencies, which have been stabilised using LQR method [24] that resulted in K(s) = 3.28s + 0.4142. Fig. 7 shows that the magnitude of v_{d-1} transforms from increasing oscillations to diminished sustained oscillation with the introduction of K(s) in the feedback loop from v_{d-1} to i_{dd-1}^* .

4.2. Current control and transient stability

Eigenvalues corresponding to the CC for DER_1 , based on the coupling matrix in (4), is presented in Fig. 8. As mentioned in Section 2, the objective of the current control design is to minimize the impact of load variation on performance of the controller. Fig. 8a shows that the eigenvalues of DER₁, with its nominal load, shift from an unstable zone to a stable one for increasing values of the gains K_{PI} and K_{II} . However, for the same K_{PI} and K_{II} gains, but with increased loading condition, the eigenvalues show unpredictable system behavior, as illustrated in Fig. 8b. Consequently, the gains have been incremented further so that the eigenvalues do not shift position by a considerable margin with varying loads, as demonstrated by Fig. 8c. This invariability of the eigenvalue positions with variations in the loading condition is essential for maintaining the relative response time of the CC with respect to the VC. Besides, the dominant eigenvalues pertaining to the CC are further left compared to that of the VC, thereby assuring faster response of the former compared to the latter. Accordingly, $\textit{K}_{PI} = 40*10^5$ and $\textit{K}_{II} =$ $108*10^5$, which generates step responses where i_{fd-1} tracks i_{fd-1}^* and is decoupled from the other inputs.

4.3. Power transfer and steady-state stability

This section demonstrates the steady-state voltage at bus no. 684 due to power transferred by DER_1 from bus no. 611, based on the analysis in Section 2.3. In conventional power system, with increasing load demand, power at the receiving end increases swiftly at first and then gradually until a maximum value is reached, which is followed by a gradual descent [25]. However, this phenomenon assumes a constant voltage source at the sending end, which is possible only if \mathbf{m}_{a-1} is constant in (5). Fig. 9 shows the steady state voltage profile at Bus 684, with a constant \mathbf{m}_{a-1} , as a function of the active power transferred to the load with increasing load demand. However, \mathbf{m}_{a-1} increases

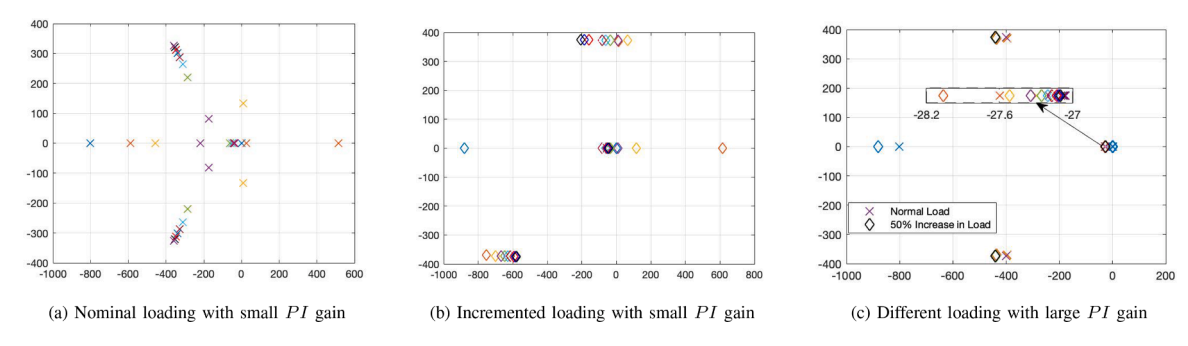


Fig. 8. Eigenvalues of current controller by varying K_{PI} and K_{II} gains under different loading conditions.

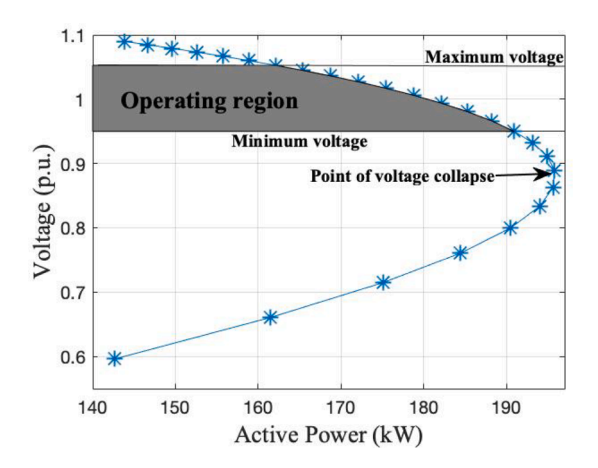


Fig. 9. Power transfer and voltage at the receiving end bus with constant amplitude modulation.

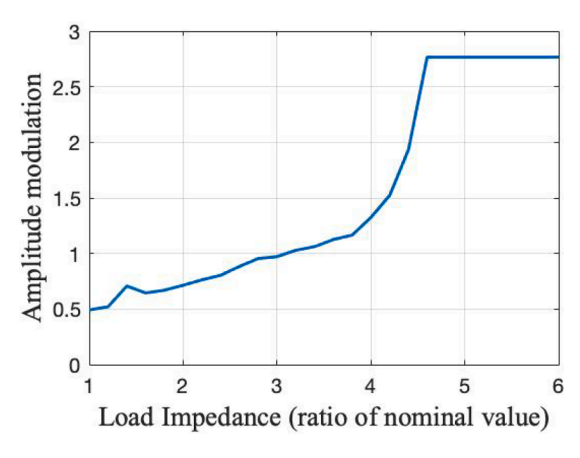


Fig. 10. Variation of amplitude modulation with load impedance.

non-linearly with increasing load demand, until the CC reaches its saturation limit, as shown in Fig. 10. Besides, DER_1 is a battery, and hence V_{dc-1} follows a discharge profile, as illustrated in Fig. 11. Accordingly, the actual receiving end voltage versus active power, for the same increase in load demand, has been demonstrated in Fig. 12. In this figure, V_{dc-1} follows only the linear region of the battery discharge curve (Fig. 11) for 95 A discharge current. A comparison between Figs. 9 and 12 shows that the power transferred for the same increment of load is more when the variation of \mathbf{m}_{a-1} is taken into account. This causes voltage rise instead of a collapse, until the battery reaches its knee voltage. Thus, the power transfer between buses must be carefully controlled in C- μ Grid. Unlike a droop controller, this problem cannot be alleviated by merely introducing virtual inertia into the control loop.

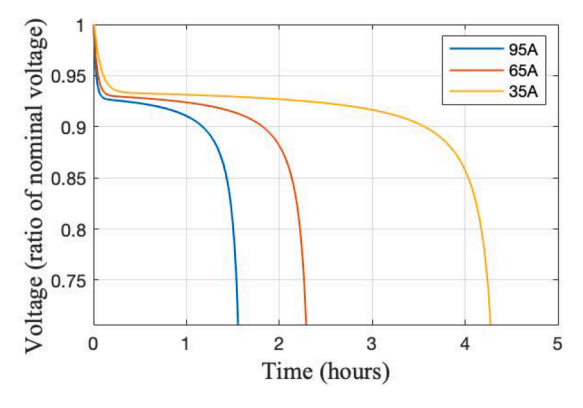


Fig. 11. Discharge profile of battery.

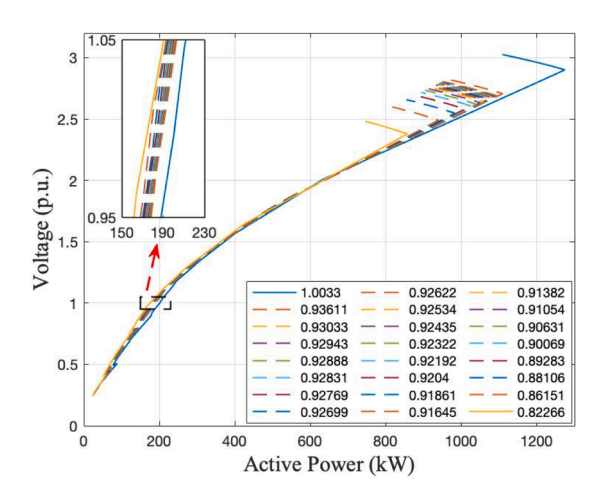


Fig. 12. Power transfer and voltage at the receiving end bus with non-linear amplitude modulation and DC voltage.

This necessitates a C-µGrid-CC, which can estimate the optimum voltage set points for the PCs based on the states of the C-µGrid.

5. Simulation results and discussion

A detailed model of the system under study has been developed in a real-time set-up using OPAL-RT, and performance of the controllers has been evaluated during normal operating conditions and in the event of delay. In the following case studies, the system has been simulated with the C- μ Grid operating in islanded mode. For each case study, the DERs receive direct axis voltage set points (v_{dk-i}^*) using two different methods, 1) Conventional OPF, and 2) The proposed CMPT method in Section 2.3. The quadrature axis voltage set points (v_{qk-i}^*) are equal to zero, since these have been used to control frequency based on Synchronous

Table 1Case1: Under normal operating condition.

	DER No.	Parameters	OPF	CMPT
1 _{Bus 611}	v_{d-1}^* (V)	4168.2	4164	
	P (MW)	0.45	0.38	
	Q (MVAr)	0.075	-0.075	
	Performance	Stable	Stable	
$2 _{Bus\ 652}$	$v_{d-2}^{*}(V)$	4160	4160	
	P (MW)	0.234	0.14	
	Q (MVAr)	-0.35	-0.378	
	Performance	Stable	Stable	
$3 _{Bus\ 692}$	v_{d-3}^{*} (V)	4160	4172.5	
	P (MW)	-0.093	0.67	
	Q (MVAr)	-0.28	0.158	
	Performance	Unstable	Stable	
4 _{Bus 675}	v_{d-4}^{*} (V)	4172.5	4172.5	
	P (MW)	1.55	1.02	
	Q (MVAr)	0.08	-0.18	
	Performance	Unstable	Stable	
	Total Losses	0.29 MVA	0.22 MVA	

Reference Frame Phase Locked Loop (SRF-PLL). The DERs have specific maximum P_k and Q_k capacities, reflecting the state of charge of batteries and irradiance received by PVs.

5.1. Test cases: Case I

In this case, the C- μ Grid accommodates a total load of 2.43 MW and 1.20 MVAr, along with VAr compensators of 0.7 MVAr. The v_{dk-i}^* provided to the DERs using OPF and CMPT, along with the corresponding system performance are summarised in Table 1. Stability of the PC of DER_1 , due to v_{d1-611}^* provided by CMPT and PC design in Section 4, is shown in Fig. 13. The quality of voltage and current injected by DER_1 at bus no. 611 is shown in Fig. 14.

However, as shown in Table 1, the VCs of DER_3 and DER_4 fail to follow their respective v_{dk-i}^* provided by OPF until the end of 15s (illustrated by the filtered signals in Fig. 15).

Consequently, the i_{fd-3} and i_{fq-4} go through a delayed zero crossing resulting in the change of direction of P_3 and Q_4 delivered by DER_3 and DER_4 , respectively. This causes additional power loss and increased harmonic injection, where THD of the $3-\phi$ current increases from 3% to 14% at these buses. Since the CCs of these DERs precisely track their respective references, inferior performance of the VCs can be attributed to the miscalculation of power transferred/received by DER_3 from its adjacent buses. Although, the controllers eventually converge by adjusting the filter currents, the system becomes vulnerable. This is demonstrated by Fig. 16, where the load at bus 692 increases by 50% at t=15s. This additional step changes drives P_3 to zero when OPF set points are used, thereby under utilizing the battery.

5.2. Test cases: Case 2

In this case, the $C-\mu Grid$ accommodates a total load of 3.08 MW and 1.63 MVAr, with the voltage set-points as shown in Table 2 and a delay of 5s at the feedback signal for DER_1 . Fig. 17 shows that the voltage controller of DER_1 fails to recover and track the OPF based reference, however, the controller rebounds within a couple of seconds for the CMPT based references. This also causes failure of the VC of DER_2 , while the other two DERs follow their respective references. As a result, the

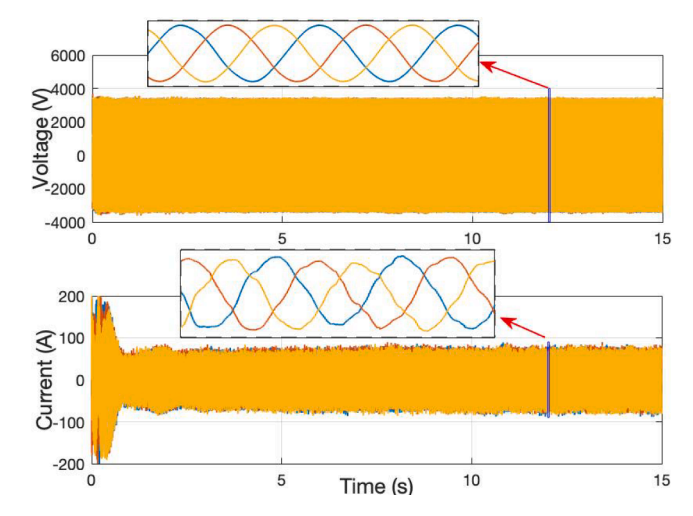


Fig. 14. Case 1: $3-\phi$ voltage and current at Bus no. 611 based on V_{d-1}^* using CMPT.

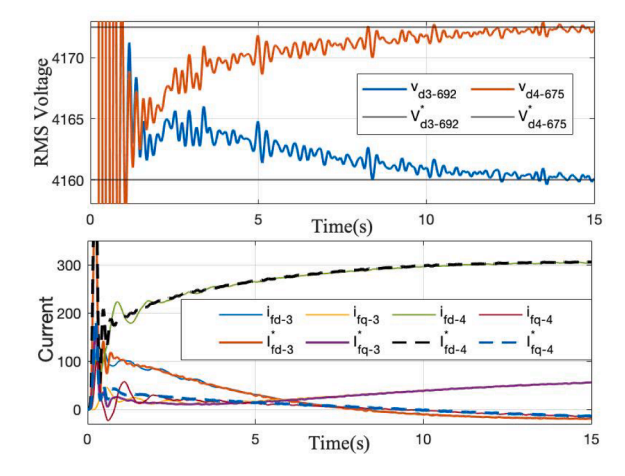


Fig. 15. Case 1: Performance of voltage and current controllers of DERs 3 and 4 for OPF based set-points.

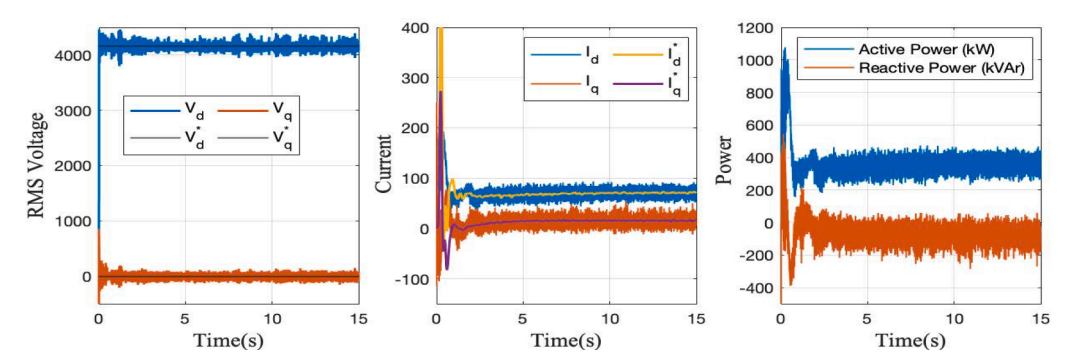


Fig. 13. Case 1: Performance of primary controllers of DER_1 with V_d^* based on CMPT.

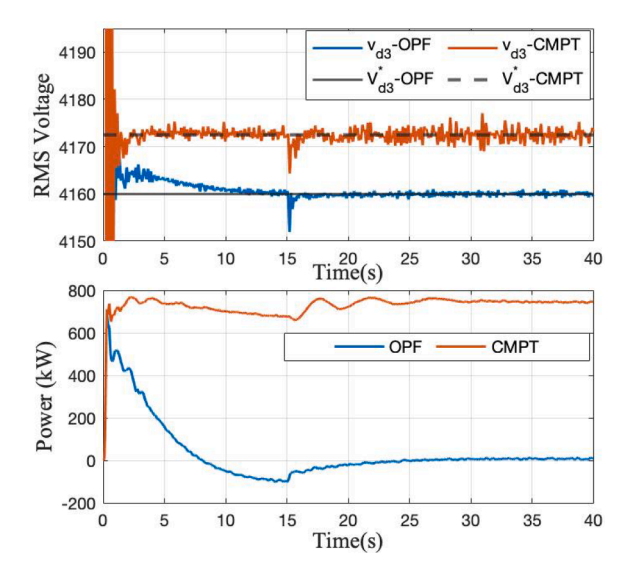


Fig. 16. Case 1 with step change in load: Performance of VC of DER_3 and active power transfer.

Table 2Case2: With 5s delay in *DER*₁.

OPF		CMPT	CMPT	
$v_{d-1}^* = 4368$ $v_{d-3}^* = 4284.8$	$V_{d-2}^* = 4368$ $v_{d-4}^* = 4284.8$	$ u_{d-1}^* = 4180.8 $ $ u_{d-3}^* = 4168.3 $	$ u_{d-2}^* = 4180.8 $ $ u_{d-4}^* = 4168.3 $	

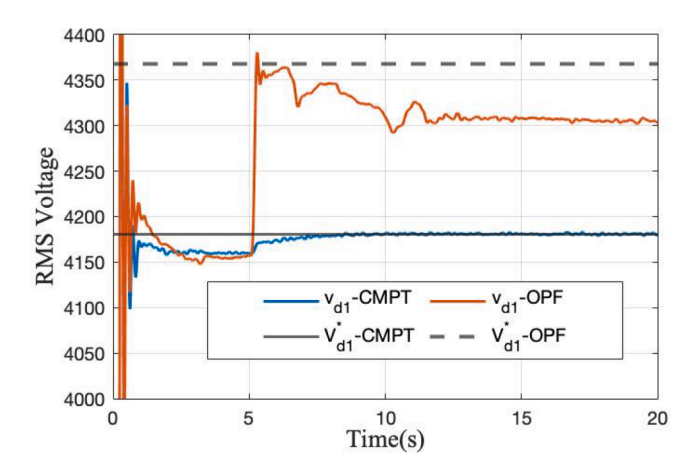


Fig. 17. Case 2: Performance of voltage controller of DER1.

CCs of DERs 1 and 2 will eventually saturate, which will cause further miscalculation of power by the C- μ Grid-CC.

6. Conclusion and future work

In this work, we have developed a control method for C- μ Grids with an emphasis on transient stability of the system in islanded mode of operation. The proposed design achieves controller stability by decoupling the state vectors of a highly coupled system at different levels of the control hierarchy. Accordingly, parameters of the VCs have been tuned based on filter design, while the same for CCs have been tuned based on the variation of equivalent load at the DER buses. The design of VCs have also incorporated communication delays, whose impact on the system has been reduced using LQR method. Besides, the relative response time of the controllers, based on their hierarchy, have been included in the control design. Our analysis shows that power transfer

between the multi-points of coupling causes voltage variation which is different from that of conventional power system. Accordingly, a power transfer method named as CMPT has been proposed, which encompasses all the dynamics of the DERs.

The PC design has been tested in a C- μ Grid structure in a modified IEEE-13 bus system, where the C- μ Grid-CC provides voltage references to the PCs based on OPF and CMPT. The simulation results show that certain combination of voltage references, which are based on OPF, have a destabilizing effect on the system due to the miscalculation of power transferred between buses. CMPT based voltage references provide better stability under normal operating condition, and improved recovery in the event of delay.

This aforementioned analysis sheds light on the functional requirements of a C- μ Grid-C/D-C. This C/D-C should be able to determine voltage references of the DERs considering accurate power transfer, DC output voltage of the DERs, provide room for system recovery during emergency, while balancing the cost with the benefits. Besides, the controller must have a fast response time so as to make real-time control decisions. Thus, the desired states of the system is known only qualitatively and not quantitatively, which makes a reinforcement learning based control algorithm with adaptive traits more suitable as the C/D-C. Our future work is development of a C- μ Grid-CC and its evaluation in a cyber-physical testbed.

CRediT authorship contribution statement

Oindrilla Dutta: Conceptualization, Data curation, Formal analysis, Investigation, Methodology, Software, Validation, Visualization, Writing – original draft, Writing – review & editing. Ahmed Mohamed: Conceptualization, Data curation, Formal analysis, Funding acquisition, Investigation, Methodology, Project administration, Resources, Supervision, Validation, Writing – review & editing.

Declaration of competing interest

The authors declare that they have no known competing financial interests or personal relationships that could have appeared to influence the work reported in this paper.

Data availability

Data will be made available on request.

Acknowledgment

This work was supported in part by the U.S. National Science Foundation under Grant 1830105 and Grant 1846940.

References

- Olivares DE, Mehrizi-Sani A, Etemadi AH, Cañizares CA, Iravani R, Kazerani M, et al. Trends in microgrid control. IEEE Trans Smart Grid 2014;5(4):1905–19.
- [2] Dragičević T, Lu X, Vasquez JC, Guerrero JM. DC Microgrids-Part I: a review of control strategies and stabilization techniques. IEEE Trans Power Electron 2015;31 (7):4876–91.
- [3] Farrokhabadi M, Cañizares CA, Simpson-Porco JW, Nasr E, Fan L, Mendoza-Araya PA, et al. Microgrid stability definitions, analysis, and examples. IEEE Trans Power Syst 2019;35(1):13–29.
- [4] Lasseter RH. Smart distribution: coupled microgrids. Proc IEEE 2011;99(6): 1074–82.
- [5] Katiraei F, Iravani MR, Lehn PW. Micro-grid autonomous operation during and subsequent to islanding process. IEEE Trans Power Deliv 2005;20(1):248–57.
- [6] Paudel A, Chaudhari K, Long C, Gooi HB. Peer-to-peer energy trading in a prosumer-based community microgrid: a game-theoretic model. IEEE Trans Ind Electron 2019;66(8):6087–97. https://doi.org/10.1109/TIE.2018.2874578.
- [7] Yuan C, Illindala MS, Khalsa AS. Co-optimization scheme for distributed energy resource planning in community microgrids. IEEE Trans Sustain Energy 2017;8(4): 1351–60. https://doi.org/10.1109/TSTE.2017.2681111.
- [8] Carter D, Saucedo D, Zoellick J, Chamberlin C, Marshall M, Shoemaker S, et al. Demonstrating a secure, reliable, low-carbon community microgrid at the Blue Lake Rancheria. California Energy Commission 2019. Available Online at: https

- ://www.energy.ca.gov/sites/default/files/2021-05/CEC-500-2019-011.pdf. Accessed: February 01, 2024.
- [9] Warneryd M, Håkansson M, Karltorp K. Unpacking the complexity of community microgrids: a review of institutions' roles for development of microgrids. Renew Sustain Energy Rev 2020;121:109690.
- [10] Wilms H, Mildt D, Cupelli M, Monti A, Kjellen P, Fischer T, et al. Microgrid field trials in sweden: Expanding the electric infrastructure in the village of Simris. IEEE Electrif Mag 2018;6(4):48–62.
- [11] Rosado SP, Khadem SK. Development of community grid: review of technical issues and challenges. IEEE Trans Ind Appl 2018;55(2):1171–9.
- [12] Dutta O, Mohamed A. Reducing the risk of cascading failure in active distribution networks using adaptive critic design. IET Gener Transm Distrib 2020;14(13): 2592–601. https://doi.org/10.1049/iet-gtd.2020.0045.
- [13] Li J, Liu Y, Wu L. Optimal operation for community-based multi-party microgrid in grid-connected and islanded modes. IEEE Trans Smart Grid 2018;9(2):756–65. https://doi.org/10.1109/TSG.2016.2564645.
- [14] Ahmad F, Alam MS, Shariff SM, Krishnamurthy M. A cost-efficient approach to EV charging station integrated community microgrid: a case study of indian power market. IEEE Trans TranspElectrif 2019;5(1):200–14. https://doi.org/10.1109/TTF_2019.2893766
- [15] Wang Y, Tang Y, Xu Y, Xu Y. A distributed control scheme of thermostatically controlled loads for the building-microgrid community. IEEE Trans Sustain Energy 2020;11(1):350–60. https://doi.org/10.1109/TSTE.2019.2891072.

- [16] Han H, Hou X, Yang J, Wu J, Su M, Guerrero JM. Review of power sharing control strategies for islanding operation of ac microgrids. IEEE Trans Smart Grid 2015;7 (1):200-15.
- [17] Dragičević T, Lu X, Vasquez JC, Guerrero JM. DC microgrids-Part I: a review of control strategies and stabilization techniques. IEEE Trans Power Electron 2016;31 (7):4876–91. https://doi.org/10.1109/TPEL.2015.2478859.
- [18] Tu J, Yin Z, Xu Y. Study on the evaluation index system and evaluation method of voltage stability of distribution network with high DG penetration. Energies 2018; 11(1):79.
- [19] Lasseter RH. Smart distribution: coupled microgrids. Proc IEEE 2011;99(6): 1074–82. https://doi.org/10.1109/JPROC.2011.2114630.
- [20] Guo X, Lu Z, Wang B, Sun X, Wang L, Guerrero JM. Dynamic phasors-based modeling and stability analysis of droop-controlled inverters for microgrid applications. IEEE Trans Smart Grid 2014;5(6):2980–7.
- [21] Loiseau JJ, Michiels W, Niculescu S-I, Sipahi R. Topics in time delay systems. Lecture notes in control and information sciences, 388; 2009.
- [22] Vyhlídal T, Lafay J-F, Sipahi R. Delay systems: from theory to numerics and applicationsvol. 1. Springer Science & Business Media; 2013.
- [23] Mohan N, Undeland TM, Robbins WP. Power electronics: converters, applications, and design. John Wiley & Sons; 2003.
- [24] Ogata K. Modern control engineering. Prentice Hall; 2010.
- [25] Kundur P, Balu NJ, Lauby MG. Power system stability and controlvol. 7. McGraw-hill New York; 1994.